The role of lateral boundary conditions in simulations of mineral aerosols by a regional climate model of Southwest Asia

Marc Pace Marcella · Elfatih A. B. Eltahir

Abstract The importance of specifying realistic lateral boundary conditions in the regional modeling of mineral aerosols has not been examined previously. This study examines the impact of assigning values for mineral aerosol (dust) concentrations at the lateral boundaries of Regional Climate Model version 3 (RegCM3) and its aerosol model over Southwest Asia. Currently, the dust emission module of RegCM3 operates over the interior of the domain, allowing dust to be transported to the boundaries, but neglecting any dust emitted at these points or from outside the domain. To account for possible dust occurring at, or entering from the boundaries, mixing ratios of dust concentrations from a larger domain RegCM3 simulation are specified at the boundaries of a smaller domain over Southwest Asia. The lateral boundary conditions are monthly averaged concentration values (μg of dust per kg of dry air) resolved in the vertical for all four dust bin sizes within RegCM3's aerosol model. RegCM3 simulations with the aerosol/dust model including lateral boundary conditions for dust are performed for a five year period and compared to model simulations without prescribed dust concentrations at the boundaries. Results indicate that specifying boundary conditions has a significant impact on dust loading across the entire domain over Southwest Asia. More specifically, a nearly 30% increase in aerosol optical depth occurs during the summer months from specifying realistic dust boundary conditions, bringing model results closer to observations such as MISR. In addition, smaller dust particles at the boundaries have a more important impact than large particles in affecting the dust loading within the interior of this domain. Moreover, increases in aerosol optical depth and dust concentrations within the interior domain are not entirely caused by inflow from the boundaries; results indicate that an increase in the gradient of concentration at the boundaries causes an increase of diffusion from the boundaries. Lastly, experiments performed using a climatology of dust concentrations yield similar results to those using actual monthly values. Therefore, using a climatology of dust mixing ratios is sufficient in implementing lateral boundary conditions for mineral aerosols. In short, this work concludes that realistic specification of lateral boundary conditions for mineral aerosols can be important in modeling the dust loading over arid regional climates such as Southwest Asia.

Keywords Mineral aerosols · Regional climate modeling · Southwest Asia · Dust · Boundary conditions

1 Introduction

Mineral aerosols, dust, have important implications in shaping both global and regional climate via effects on radiation and clouds, and ultimately temperature and precipitation (Miller and Tegen 1998; Sokolik et al. 2001; Solmon et al. 2008; Zhang et al. 2009) Yet, the importance of specifying dust concentrations at the lateral boundaries in regional modeling has not been examined in the literature. Although many models, both global and regional, perform satisfactorily in simulating dust episodes, many constrain dust emissions with tuning parameters (Tegen

M. P. Marcella (✉)
Department of Civil and Environmental Engineering,
Ralph M. Parsons Laboratory, Building 48-216, MIT,
77 Massachusetts Avenue, Cambridge, MA 02139, USA
e-mail: marcpace@mit.edu

M. P. Marcella · E. A. B. Eltahir
Massachusetts Institute of Technology,
Cambridge, Massachusetts

and Miller 1998; Cakmur et al. 2004). Likewise, in Regional Climate Model version 3 (RegCM3), the dust scheme does not simulate dust emissions over the outer-most point in both lateral directions. Although, dust and other aerosols may be transported to these strips, dust originating from these regions, and those outside, are unaccounted for. As a result, it is possible that neglecting mineral aerosols at the boundaries may result in an underestimation of dust loading within the interior domain as seen in Marcella and Eltahir (2010). Here we specify dust concentrations at the boundaries of a RegCM3 simulation covering most of Southwest Asia provided by a larger domain simulation that spans from the Atlantic Ocean in the west to the Indian Ocean in the east. Therefore, this study provides insight into how sensitive regional dust and climate models are to the specification of mineral aerosols at the boundaries.

2 Model description and observational datasets

2.1 Regional climate model version 3

In this study, Regional Climate Model version 3 (RegCM3) is used to simulate the dust loading over the semi-arid region of Southwest Asia. Several studies have been completed using RegCM3, as referenced in Giorgi et al. (1998). Originally developed at the National Center for Atmospheric Research (NCAR) and now maintained at the International Center for Theoretical Physics (ICTP), RegCM3 is a three-dimensional, hydrostatic, compressible, primitive equation, σ vertical coordinate, regional climate model (RCM). RegCM3 maintains much of the dynamical core of NCAR/ Pennsylvania State University's mesoscale model, MM5 (Grell et al. 1994). The model now employs NCAR's Community Climate Model (CCM3) radiative transfer package (Kiehl et al. 1996). In addition, land surface physics are modeled by the Biosphere-Atmosphere Transfer Scheme (BATS1e) of Dickinson et al. (1993), while boundary layer physics are modeled by Holtslag et al. (1990) non-local planetary boundary layer scheme (Giorgi et al. 1993a). RegCM3 also employs Zeng's bulk aerodynamic ocean flux parameterization, where sea surface temperatures (SST's) are prescribed (Zeng et al. 1998). In addition, three different convection schemes (Kuo, Grell, and Emanuel) are available for non-resolvable rainfall processes (Giorgi et al. 1993b). After some experimentation with other convection schemes, the Kuo scheme best simulated the magnitude as well as spatial distribution of winter rainfall and thus was chosen for our experiments (Marcella and Eltahir 2008). Lastly, RegCM3 includes a large-scale, resolvable, non-convective moisture scheme, the sub-grid explicit moisture scheme-SUBEX (Pal et al. 2000) The authors refer readers to Pal

et al. (2007) for the most recent developments and description of RegCM3.

2.2 Desert dust module and aerosol model of regional climate model version 3

RegCM3 features a fully coupled aerosol chemistry model including a radiatively-active dust module for semi-desert and desert model grid-cells (Zakey et al. 2006). In this study, we used an updated version of the Zakey et al. (2006) dust module. In this scheme, dust emissions are strongly dependent on wind speed, surface characteristics, and soil particle size. Following the work of Marticorena and Bergametti (1995) and Alfaro and Gomes (2001), the dust emission calculation is based on empirical parameterizations for both soil aggregate saltation as well as sandblasting processes. Dust emissions within the scheme follow four basic steps: (1) Specification of soil aggregate size (D_p) based on a three-mode lognormal distribution determined by the soil texture class, (2) calculation of a minimum threshold friction velocity based on empirical parameterizations of Marticorena and Bergametti (1995), (3) calculation of the horizontal saltating soil aggregate mass flux, $dH_F(D_p)$, defined as:

$$dH_F(D_p) = E * \frac{\rho_a}{g} * u^{*^3} * \left(1 + R(D_p)\right) * \left(1 - R^2(D_p)\right)$$
$$* dS_{rel}(D_p) \tag{1}$$

where, E is the ratio of the erodible to total surface, ρ_a is the density of air, g, gravity, u^* is the wind friction velocity, $R(D_p)$ is the ratio of the minimum threshold friction velocity to the actual friction velocity and $dS_{rel}(D_p)$ is the relative surface of soil aggregate of diameter D_p, and (4) calculation of the vertically transportable dust particle mass flux generated by the saltating aggregates. A portion of the horizontal saltation flux is proportioned to a kinetic energy flux. From here, the vertical flux of the soil aggregates is determined via binding energies and the aforementioned kinetic energy. Lastly, transport bins for different dust particle sizes are used for advection and deposition (both wet and dry) of dust particulates following the chemical tracer model in RegCM3. Furthermore, the tendency of any tracer, χ is modeled as:

$$\frac{d\chi}{dt} = -\bar{V} \cdot \nabla\chi + F_H + F_V + T_C + S - R_{W_{ls}} - R_{W_c} - D_d$$
$$+ \sum \left(Q_p - Q_l\right) \tag{2}$$

where, $-\bar{V} \cdot \nabla\chi$ is the advection of the tracer in the horizontal and vertical, F_H and F_V are diffusion in the horizontal and vertical (a function of wind speed and horizontal/vertical concentration gradient), T_C is convective transport, S is the source term, $R_{W_{ls}}, R_{W_c}$ are wet

removal from large scale and convective precipitation, respectively, D_d is dry deposition and $\sum (Q_p - Q_l)$ is the physio-chemical production and loss of the tracer. The four bin sizes for transport and removal via Eq. 2 are: 0.01–1.0, 1.0–2.5, 2.5–5.0 and 5.0–20.0 μm (Zakey et al. 2006). Over Southwest Asia's summer desert climate, the key processes in determining the tendency of dust are advection, diffusion, sources, and dry deposition.

2.3 NASA's multiple-angle imaging spectroradiometer

Launched on NASA's Terra satellite Earth Observing System mission, the Multi-angle Imaging Spectroradiometer (MISR) retrievals are compared to model simulations of aerosol optical depth values. MISR contains nine cameras that observe the Earth at nine different viewing angles and four different bands. In this study, MISR Level 3 Component Global Aerosol Product, at $0.5° \times 0.5°$ resolution, is used for AOD values at 555 nm. The temporal coverage used in this analysis follows that of the RegCM3 simulations, from 2000–2004. For further information on the MISR dataset, the authors refer the reader to Kahn et al. (2009).

3 Experimental design

3.1 Domain setup

Simulations using RegCM3 were completed for 5 years spanning from 2000 through 2004 with a one year model spin-up time. The domain, centered at 31°N, 44.5°E at 30 km resolution, has 88 points in the zonal and 74 points in the meridional direction using a Lambert Conformal projection. The domain covers most of Southwest Asia from the Mediterranean and Caspian Seas in the north to the Red Sea and Oman in the south. Fig. 1 represents the model domain, topography, and land use in all simulations. As examples of three different scales, areal averages are calculated over the country of Kuwait (46.5°E–48.5°E, 28.4°N–30.2°N), a boxed region (23.5°E–33.5°E, 40°N–50°N) and the entire domain, as shown in Fig. 1. Initial and boundary conditions to drive the atmospheric model are implemented from the National Center for Environmental Prediction/National Center for Atmospheric Research (NCEP/NCAR) Reanalysis Project 2—NNRP2 of Kalnay et al. (1996). Lateral boundary conditions (LBC's) are enforced by applying the exponential relaxation of Davies and Turner (1977). As mentioned prior, SST's are prescribed to RegCM3 from the National Oceanic and Atmospheric Administration (NOAA) optimally interpolated SST (OISST) dataset of Reynolds (2002). The SST datasets are $1° \times 1°$ monthly resolution and are based on in situ and satellite observations.
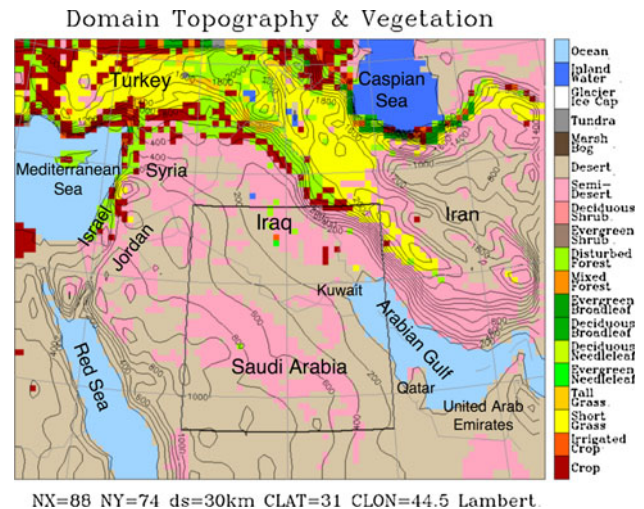

Fig. 1 Domain implemented for all simulations with topography contoured (200 m intervals) and vegetation shaded. A significant portion of the domain is classified by semi-desert or desert landcover at 30 km

3.2 Simulations description

A total of three different RegCM3 simulations are performed with two configurations of dust boundary conditions in RegCM3. The control, CONT, provides a baseline simulation using the components of the model listed above with RegCM3's aerosol and dust emission model but without representation of dust at the boundaries. BC contains the same setup as CONT but includes monthly averaged mixing ratios for each dust tracer imposed at the boundaries. Lastly, the CLIMABC simulation uses a "climatology" (averaged across the 5 years of boundary condition data) for monthly values of dust concentrations. To discern the effects of boundary conditions on dust loading, initial comparisons are made between CONT and BC simulations. Then, to determine if using a climatology for boundary conditions is sufficient, results from BC are compared to CLIMABC. Table 1 provides a complete summary of simulations performed.

3.3 Implementation of dust boundary conditions

First, a five year simulation with RegCM3 over a large domain covering most of Africa in the west, Europe in the north, Pakistan in the east, and the Indian Ocean in the south is completed at 30 km horizontal resolution using the dust and aerosol modules of RegCM3 with matching physics of the CONT simulation (Fig. 2). The resulting dust mixing ratios from this simulation for all four dust tracer bin sizes are imposed at the boundaries of the smaller domain (see Fig. 2). The concentrations are two-dimensional (X-Z or Y-Z), averaged values (μg dust kg^{-1} air) for each month of each corresponding simulation year (Fig. 2).

Table 1 Summary of simulations performed for the period of 2000–2004

Simiulation	Description of processes included
CONT	No boundary conditions for dust
BC	Monthly averaged dust mixing ratio at boundaries
CLIMABC	Climatology of dust boundary conditions

All simulations use NNRP2 lateral boundary conditions and OISST prescribed sea surface temperatures. These names will be used to reference each simulation in the text

The values are set at the outermost point of the domain for the corresponding boundary (north, south, east, west) in each vertical level (eighteen levels in total). There is no relaxation used for the boundary values; that is, the dust concentration is placed only at the boundary point and does not directly influence adjacent points. Similarly, the "climatology" boundary dataset is constructed by using the average value for each month calculated from the five values of each month in the five year period. For example, the August climatology value is constructed by taking the value of August from each year (2000, 2001, 2002, 2003, and 2004) and then calculating the mean value for August.

4 Results and discussion

4.1 Effects of boundary conditions on aerosol optical depth

The effects of including mineral aerosols at the boundaries are presented in Fig. 3. Shown is the mean summertime (June, July, August) aerosol optical depth (AOD) for CONT, BC, and CLIMABC. As seen in Fig. 3, large increases in dust loading occur throughout the domain, particularly over the southern and eastern portions of the domain. For example, AOD values across eastern Iran nearly double from 0.1 to 0.2 (compare Fig. 3a,b). Likewise, across the United Arab Emirates (UAE), AOD values increase by over 65% when including boundary conditions. However, changes over the western and northern boundaries are nearly negligible. These results are logical since dust concentrations at the south and east boundaries are significantly larger than those in the north and west in the large domain (see Fig. 2). Larger values are found in the east and south since these areas contain dust sources at or just outside the smaller domain's boundaries. As documented in Prospero et al. (2002), Oman and the Arabian Peninsula are well known, pronounced dust sources as is the basin between Iran and Afghanistan. These sources are not captured within the dust model but are now represented via dust concentrations transported at the boundaries. Nevertheless, the resulting increase in JJA AOD averaged across the domain is nearly 30% and has a distinct positive northwest to southeast gradient as shown in Fig. 4. Significant increases in dust loading (AOD difference >0.1) occur across the eastern and southeastern portions of the domain resulting in values 50 to 100% larger in BC than CONT (see Fig. 4a,b). However, as expected, in the interior of the domain, the effects of dust boundary conditions are diminished. For example, over Kuwait, AOD increases are closer to 15% with smaller increases throughout Iraq and northern central Saudi Arabia (Fig. 4b). It is important to note that large percent increases across the Mediterranean are a result of exceedingly small values of AOD there

Fig. 2 Schematic illustrating how boundary conditions are taken from large simulation in a one-way nesting manner and imposed at the boundary of the SW Asia domain. *Plotted* is total summer dust concentration ($\mu g\ kg^{-1}$) in both simulations as well as an example cross section (Y-Z) of tracer1 boundary conditions
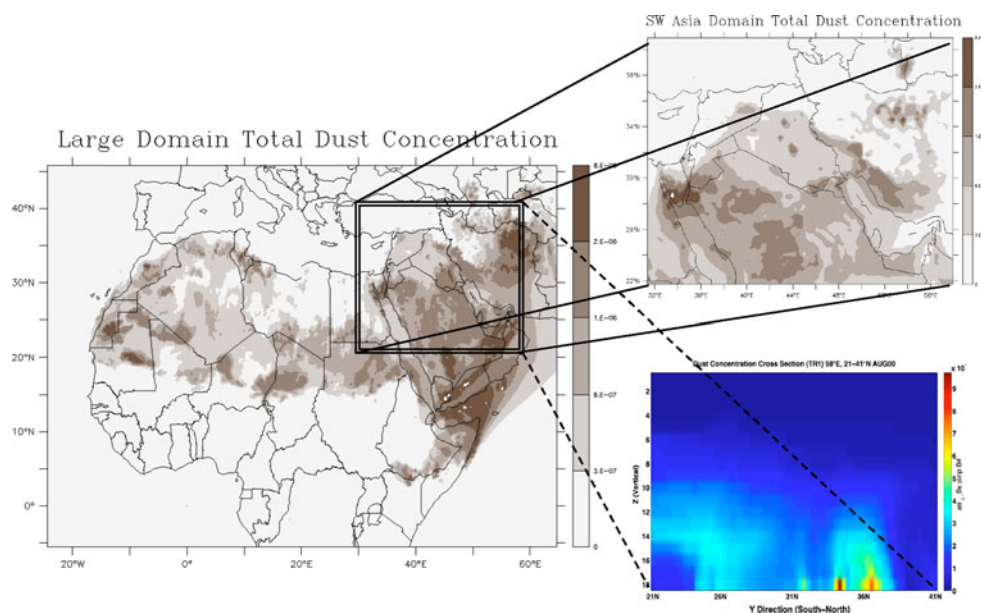
Fig. 3 Simulated average daily
summertime (JJA) AOD in
a CONT **b** BC **c** CLIMA and
d MISR observations for the
period of 2000–2004. Note areal
averages over Kuwait, the *boxed
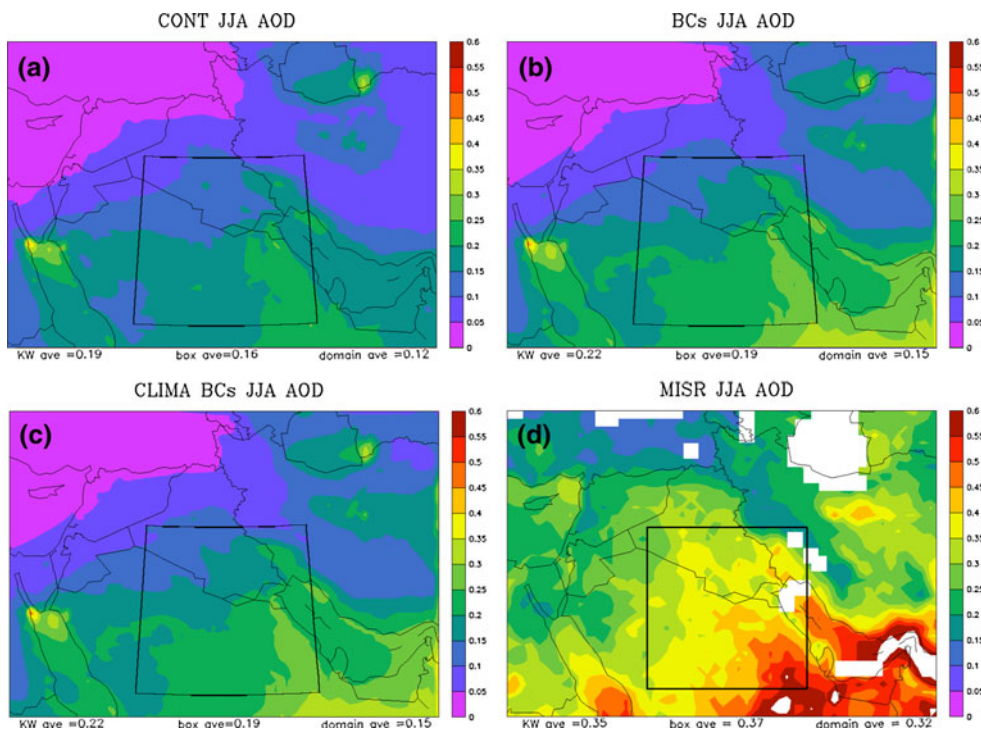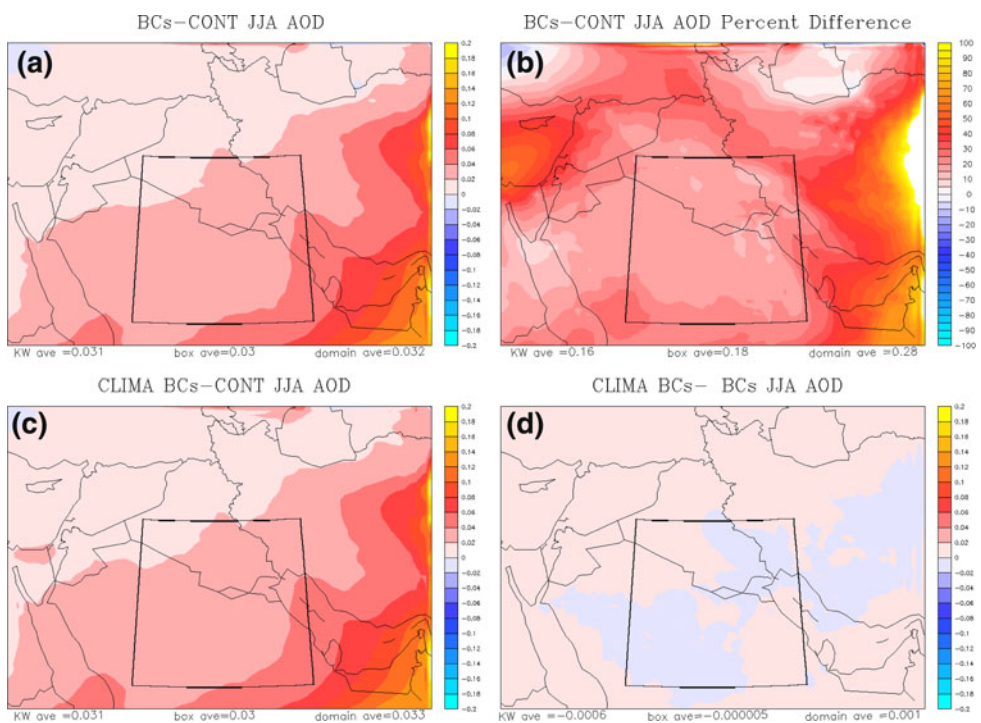region*, and the domain are also
shown

Fig. 4 Differences in RegCM3
simulated average summer
AOD between **a** BC-CONT
c CLIMABC-CONT and
d CLIMABC-BC. Also shown
in **b** is the percent difference
between BC-CONT AOD. Note
areal averages over both
Kuwait, the *boxed region*, and
the domain are also shown

to begin with (<0.05), therefore results from this region are not significant. Lastly, in the large domain, which provides the boundary conditions, domain averaged AOD is approximately 20% higher than that in the BC simulation (0.20 vs. 0.15, respectively). However, windspeeds in the larger domain are higher causing the remaining differences in dust loading between the two simulations.

Examining the seasonal effects of dust over Southwest Asia yields similar findings to spatial differences (see Fig. 5). In general, strong seasonality in AOD occurs over Southwest Asia where a maximum in optical depth is reached in April and maintained throughout the dry summer months before subsiding in mid-fall (October). That is, values of AOD in summertime are nearly 70% larger than
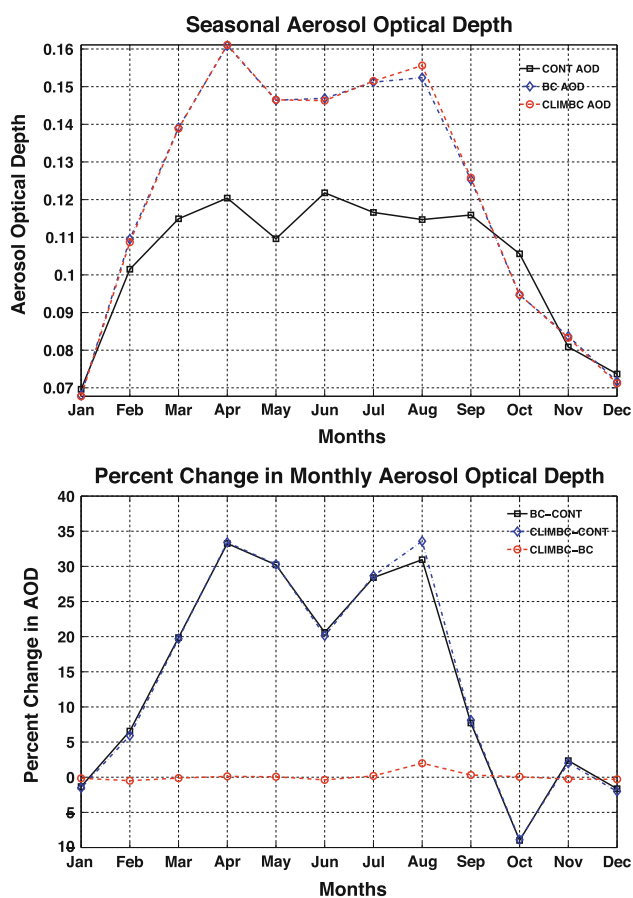
Fig. 5 Seasonal cycle and percent change in seasonal cycle of aerosol optical depth averaged over Southwest Asia for CONT, BC, and CLIMABC simulations

those found during the region's wet winter season (DJF). These model results are validated by the findings of Prospero et al. (2002), which used the observational Total Ozone Mapping Spectrometer Aerosol Index to delineate seasonality in dust emissions globally. Nevertheless, including boundary conditions results in a twenty to thirty percent increase in AOD during the entire dusty season of April through September (Fig. 5b). Therefore, interestingly, including boundary conditions causes an increase in seasonality as shown in Fig. 5a. That is, percent increases in September of only 7% and a slight decrease in October, lead to a more defined peak in dust loading. As expected, changes from November through February are nearly negligible as dust emissions are small during the relatively wet season of this region.

Consequently, including dust at the boundaries improves model performance against observations. Here we compare simulated mean daily summertime AOD to MISR measurements. NASA's MISR product is superior in capturing optical depths over desert regions compared to other instruments such as the Moderate Resolution Imaging

Spectroradiometer (Abdou et al. 2005; Prasad and Singh 2006; Marcella and Eltahir 2010). As seen in Fig. 3, aerosol optical depth values from CONT are significantly smaller than those from MISR (more than 60% less in domain average). Likewise, CONT does not adequately capture the spatial variability of AOD as seen in MISR. For example, CONT lacks the pronounced increase in AOD from northwest to southeast across the region as seen in MISR observations (Fig. 3d). Although not completely accounting for the large bias in aerosol optical depth, BC does reduce the underestimation in optical depth by 10%. More importantly, RegCM3 now has a more distinct gradient in AOD matching that of MISR observations with the domain maximum located over the UAE and southeastern Saudi Arabia. We refer the readers to Marcella and Eltahir (2010) for a more thorough examination of the performance of RegCM3's dust model over this region. This work found that a large remainder in AOD differences (between thirty and forty percent) can be resolved by including wind variability, or gustiness, in the dust emission scheme. However, some of this underestimation in AOD values may be a result of large differences in sampling time/sizes between RegCM3 and MISR. Where RegCM3 dust output is calculated every three hours, MISR retrievals occur once a day or once every other day and occur over narrow swaths meaning sampling of dust events may not be complete. Therefore, it is possible that some of the discrepancy may come from a rather coarse sampling size by the satellite compared to modeled fields.

Lastly, it should be noted that the importance of including realistic boundary conditions is a function of both model domain setup and physical region. For example, including values of dust at the boundaries for the large domain would most likely have a negligible effect on dust loading in the interior since most dust sources would be captured. Likewise, including prescribed dust mixing ratios for a domain that includes all of Australia, where most dust sources are internal, would also result in minimal dust loading changes. However, over regions where dust is transported into the domain, such as Southwest Asia, or in cases where including the entire domain is computationally onerous, (e.g., including all of Africa) supplying boundary conditions for dust values may be an acceptable alternative.

### 4.2 Changes in tracer concentrations and emission rates

Further work is completed in examining changes of actual dust tracer concentrations when including boundary conditions. As mentioned prior, dust is broken up into four bins based on particle size for transport and removal via Eq. 2: 0.01–1.0, 1.0–2.5, 2.5–5.0 and 5.0–20.0 μm (Zakey et al. 2006). Therefore, boundary conditions are implemented for each suspended mineral aerosol bin. Here we

investigate changes in the smallest (tracer1) and the largest (tracer4) dust bins.

Shown in Fig. 6 are the mixing ratios for tracer1 (0.01–1.0 μm) and tracer4 (5.0–20.0 μm) in both CONT and BC simulations. It is clear from comparing Fig. 6a to 7c, that tracer1 is transported significantly downwind from where it is emitted. In contrast, tracer4, which is larger and therefore heavier, has a higher concentration in the atmosphere (compare Fig. 6a to e). Consequently, tracer4 is not advected nearly as far from its emission sites due to larger dry deposition or gravitational settling out of the atmosphere (compare Figs. 6e to 7e). Also apparent is the similarity between changes in tracer1 concentrations and changes in AOD (see Figs. 4a and 6c). In both fields, a pronounced increase in values occurs from west to east with a maximum over the southeastern corner of the

Fig. 6 *Vertically* integrated mean summertime concentrations (μg kg^{-1}) of tracer1 and tracer4 in CONT (**a,e**) and BC (**b,f**). Also shown are differences and fractional differences between BC and CONT for tracer1 and tracer4 (**c,d,g,h**) *White* values are those larger than the color scale
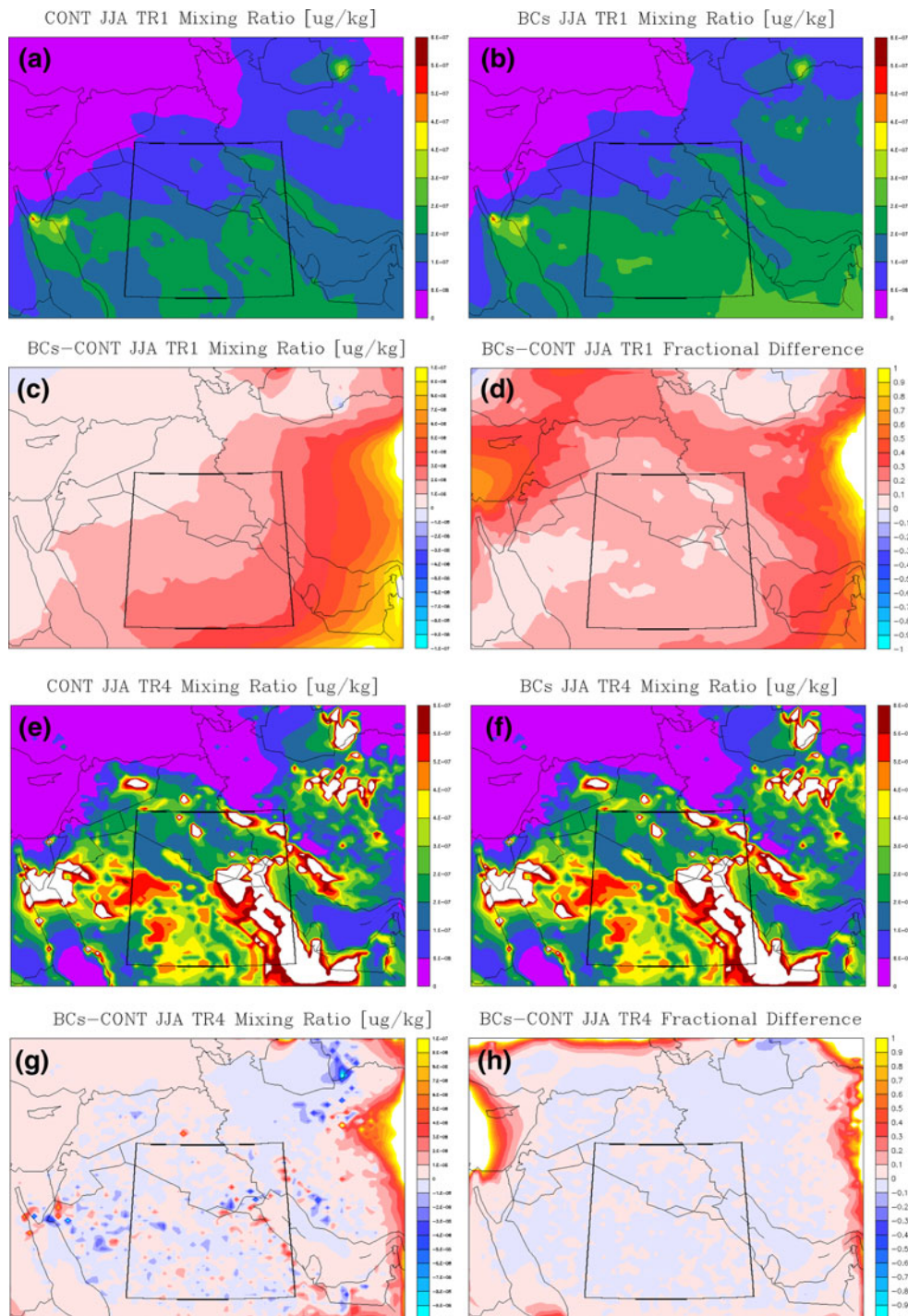
domain. For example, including tracer1 at the boundaries results in a nearly 20% increase of its concentration over the domain with significantly larger values over eastern Iran and the southern Arabian Gulf (Fig. 6d). Nevertheless, this high correlation between changes in tracer1 and changes in AOD patterns is expected given the first bin size is the most optically active of all the bins at 0.55 microns. In contrast, little change in tracer4's mixing ratio occurs when imposing boundary conditions (compare Figs. 6e to f and 6g to c). This result follows the spatial dispersion of the tracer. That is, given tracer4 is not easily advected, all marked changes occur in close proximity to the actual boundaries (Fig. 6h). This result is further confirmed by comparing the ratio of dry deposition to column mass loading for each tracer (not shown). Throughout the year, values of the ratio range from 1–10 for tracer4 whereas tracer1 values are two orders of magnitude smaller (0–0.01). That is, the amount of tracer4 that falls out normalized by the mass that is in the column of air, is nearly

one hundred times larger than tracer1. This result further solidifies the larger importance of tracer1 than tracer4 in boundary condition representation. As a result, it can be inferred that heavier dust particles are significantly less affected by boundary specification.

Lastly, comparisons of emission rates and wind fields are completed between CONT and BC simulations. As expected, differences in wind speeds and directions between the two simulations are negligible (see Fig. 7). Consequently, differences in emission rates between CONT and BC for both tracer1 and tracer4 are small (see Fig. 7). It is important to note that although 10 meter winds are plotted, wind fields for the lowest five layers of the atmospheric model (where highest dust concentrations exist in the boundary conditions) are similar to those at 10 meters. Nevertheless, the lack of difference in emission rates at the surface confirms that changes in boundary conditions are causing increases in dust concentrations and ultimately changes in AOD values throughout the domain.

Fig. 7 Average summertime wind speed (m s^{-1}) and direction in **a** CONT and **b** BC. Also shown are summertime surface emission rates (µg m^{-2}s^{-1}) for tracer1 (**c,d**) and tracer4 (**e,f**) in CONT and BC simulations. *White* values are those larger than the color scale
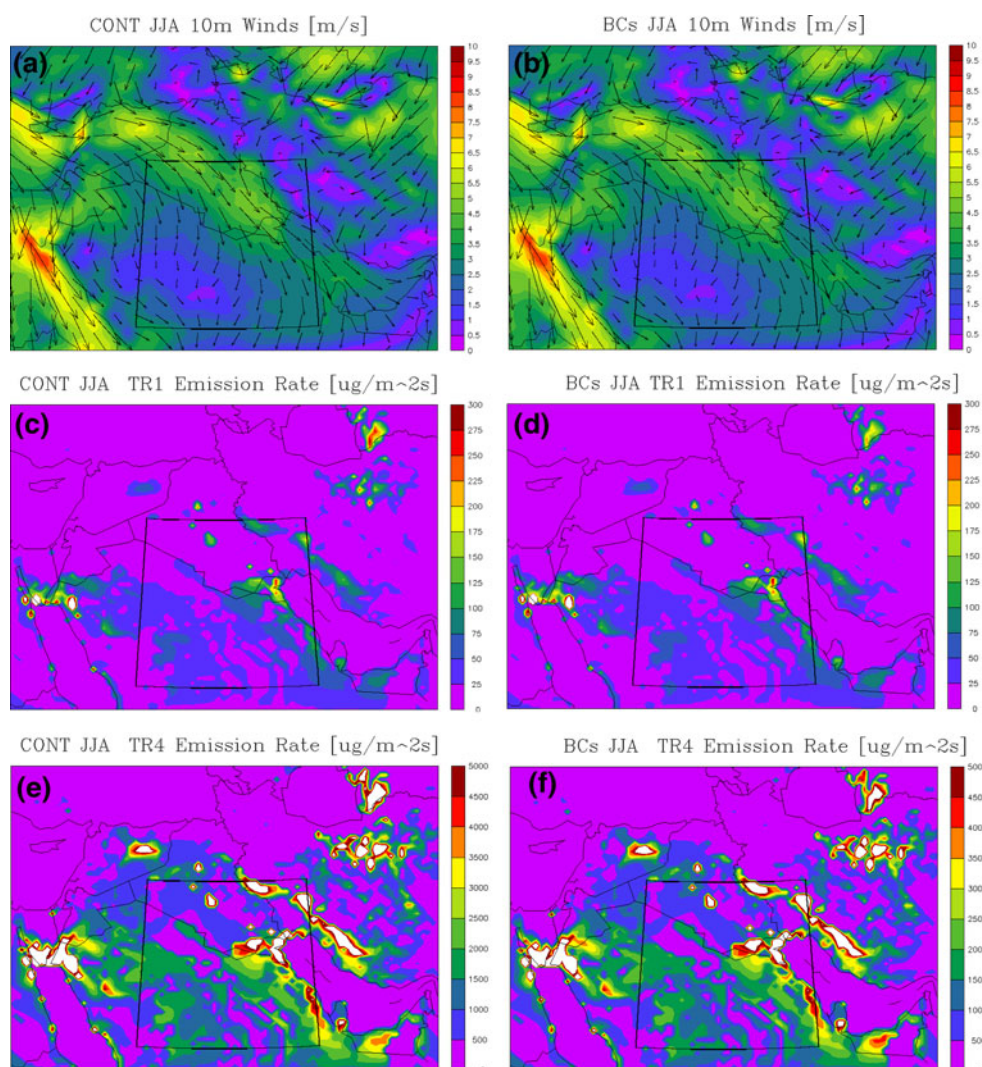
In addition, a closer inspection of the wind fields reveals that the west, north, and east are inflow boundaries where the south has wind vectors blowing out of the domain—an outflow boundary (see Fig. 7b). Small dust concentrations at the west and north boundaries make these insignificant dust inflow sources (see Fig. 2). However, large concentrations along the eastern boundary combined with winds blowing into the domain make this an important boundary for dust advection. As seen in plots of AOD and tracer1 concentrations, this region does experience dust blowing in from the northern boundary in Iran down to the UAE. Unlike the eastern boundary, the southern boundary is an outflow region yet still has a significant increase in dust loading. The increase can be attributed to an increase in the horizontal gradient of dust close to the boundary resulting in increased diffusion into the domain. As shown in Eq. 2, the tendency of a tracer is a function of both advection and diffusion, both which are a function of the concentration gradient. With a larger gradient over this region, more dust is diffused from the boundaries into the domain. Therefore, dust is transported further north as seen in Figs. 4a and 6c.

4.3 Effects on shortwave radiation and two meter temperature

It is well known that as dust particulates are suspended into the atmosphere, incoming shortwave radiation is either scattered or absorbed depending on the particulate size (Tegen and Lacis 1996; Miller and Tegen 1998). In a dust-radiation model, the nature of shortwave absorption versus shortwave reflection is strongly dependent on the refractive index used (see Zakey et al. 2006). In this model, it is found that dust particles reflect more than absorb (Zhang et al. 2009; Marcella and Eltahir 2010) shortwave radiation. For example, Zhang et al. (2009) found a nearly 5 to 10 $/m^2$ negative top of atmosphere radiative forcing caused by dust loading over East Asia. Therefore, given that including boundary conditions increases dust loading over the domain of Southwest Asia, it is expected that shortwave incident values may be reduced by further reflection or absorption. This attenuation of surface shortwave is clearly

noticeable in Fig. 8a. Similar to the spatial signature of aerosol optical depth and dust concentration increases, a decrease in shortwave radiation on the order of 5 to 10 W/m^2 is visible across the eastern and southern boundary of the domain. However, across the entire region, the overall effect is significantly less at only $2W/m^2$.

Nevertheless, with decreased shortwave radiation reaching the surface, temperatures near the surface (two meters) may be reduced. Shown in Fig. 8b is the difference between two meter temperatures in CONT and BC simulations. As seen, there is very little reduction in temperatures. A slight cooling is evident over the United Arab Emirates, southeastern Saudi Arabia, and central Iran, but these values are on the order of only 0.1–0.2°C. It should be noted, again, that dust also absorbs shortwave radiation and traps upwelling longwave radiation, depending on particle size (Tegen and Lacis 1996); consequently, dust causes some heating aloft in the dust layer (Miller and Tegen 1998). These processes are noticeable in RegCM3 and most likely help mute the cooling signal at the surface. Likewise, although shortwave radiation reaching the surface decreases by nearly 10 W/m^2 in some regions, the difference (or decrease) in the amount absorbed at the surface is less (by about 30%) due to large surface albedo over this bright desert region. This factor may help explain why the increased shortwave attenuation does not result in much cooling over the eastern portion of the domain.

4.4 Using a climatology for boundary conditions

After examining the fluctuation in dust concentration at the boundaries, it is found that the dust mixing ratios do not vary significantly from year to year (see Fig. 9). For example, at the eastern boundary, the differences between maximum and minimum JJA tracer1 concentrations in both the control simulation and the actual boundary conditions are less than 15% of the mean value (Fig. 9). Therefore, additional simulations were performed using a "climatology" of dust concentrations instead of actual values for each month. That is, the five year monthly mean values were averaged across all years for each month and then

Fig. 8 Differences in mean summertime **a** shortwave incident radiation (W m^{-2}) and **b** two meter temperature (°C) in BC and CONT simulations
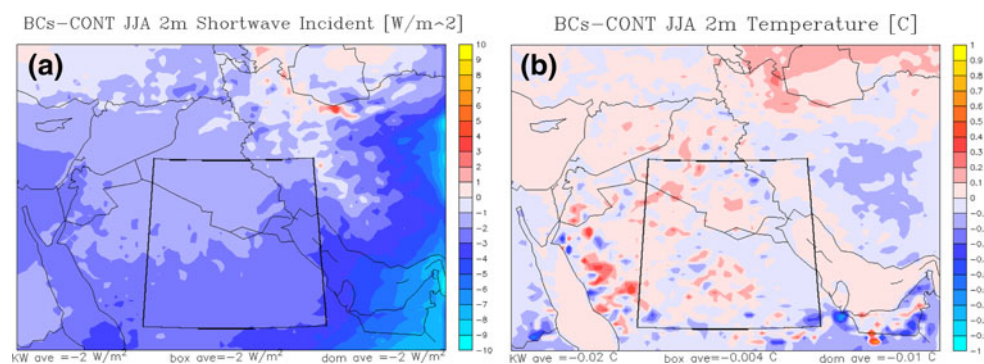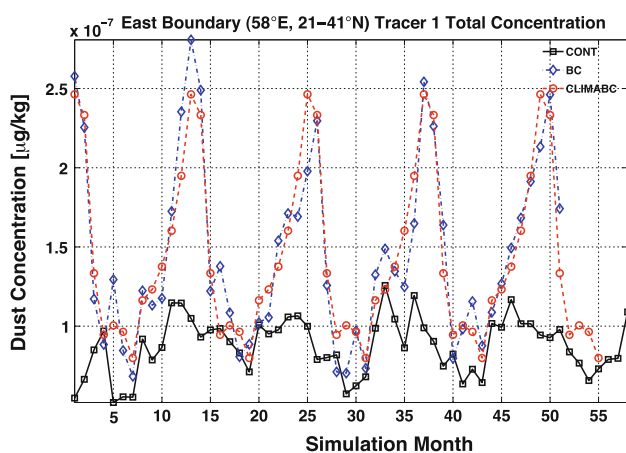
Fig. 9 *Vertically* integrated tracer1 dust concentration ($\mu g\ kg^{-1}$) for the eastern boundary (averaged in the Y, north-south, direction) for CONT, BC, and CLIMABC simulations

used for each specific month. For example, an average August dust concentration (for each tracer bin) was calculated based on the 2000–2004 data and then used for each year's August from 2000 to 2004. Figure 9 illustrates what these concentrations look like in comparison to the BC method. Results from such an experiment highlight the importance of using a nesting technique (as performed above) or whether a climatology dataset such as that from Luo et al. (2003) is sufficient in representing mineral aerosols at the boundaries. Comparing Fig. 3b to c reveals that CLIMABC's mean summertime AOD is nearly identical to that of BC. This result is further seen in Fig. 4c where a similar west to east and north to south increase in AOD occurs when using the climatology dataset. The actual difference between CLIMABC and BC's mean AOD values are plotted in Fig. 4d. Across the entire domain, differences in optical depth are insignificant (less than 1%). As expected, the results are similar when examining changes in actual tracer concentrations as well (not shown). Lastly, a closer look at the seasonality of AOD (Fig. 5a) confirms that using a climatology for dust concentrations is satisfactory; nearly no difference occurs between BC and CLIMBC monthly optical depth values across the entire year. Figure 5b confirms these results by showing that the percent difference between BC and CLIMABC in domain averaged AOD is less than three percent for any given month. Therefore we conclude that using a climatology dataset of mineral aerosols suffices in representing dust concentrations at the boundaries.

5 Summary and conclusions

Using Regional Climate Model version 3, the importance of including dust boundary conditions for simulating

mineral aerosols in a regional climate model is investigated over Southwest Asia. Currently, RegCM3 allows mineral aerosols to be transported to the boundaries, but neglects dust emissions at these locations or sources located just outside the domain. Omission of dust at these points has pronounced effects on dust loading in the domain due to inflow at the boundaries or diffusion into the domain. Here dust concentrations simulated from a larger domain covering most of Africa, southern Europe, and west Asia are imposed at the boundaries of a smaller domain over Southwest Asia. The boundary condition dataset is comprised of monthly, averaged mixing ratios (kg dust/ kg air) for the four dust bin sizes currently used in RegCM3's aerosol and dust modules.

Results indicate that specification of dust concentrations at the boundaries significantly affects dust loading over most of Southwest Asia. For example, including dust at the boundaries results in nearly a 30% increase in mean AOD values across the domain with some regions in eastern Iran and the UAE seeing nearly a 75% increase in AOD. Similarly, the spatial pattern of dust loading is affected as a more pronounced northwest to southeast gradient in both AOD and tracer mixing ratios occurs. As a result, both of these patterns bring model simulations closer to MISR observations over this region. Nevertheless, a significant underestimation in dust loading over Southwest Asia still occurs in RegCM3. Additional work completed indicates that including variability in wind speed (i.e. gustiness) helps further reduce this bias (Marcella and Eltahir 2010). Moreover, including boundary conditions causes a more pronounced seasonality (larger increases of summer AOD than winter AOD) in RegCM3 simulations. This result is consistent given the lack of much dust emissions surrounding this region during the winter months. Additionally, it appears that lighter, or smaller, dust particles at the boundaries have a more profound effect on dust loading within the domain. That is, changes in AOD parallel changes in tracer1's concentration whereas larger particles (i.e. tracer4) fall out of the atmosphere quicker; therefore, tracer4 is not advected or transported as far as tracer1. Nevertheless, the largest changes in dust loading occur in the eastern and southern boundaries, where larger boundary concentrations can be found. However, the changes are the result of two different processes. In the east, over Iran, large increases are the result of this boundary's inflow properties—winds blowing into the domain cause dust at the boundary to be blown over eastern and central Iran, dust advection. In contrast, the southern boundary has winds blowing out of the domain yet boundary condition simulations have larger aerosol optical depths over this region. Here, an increase in the dust close to the boundary causes diffusion into the domain. Thus, a buildup in mineral aerosols occurs across central Saudi Arabia. Further

work was completed in examining changes in model meteorology and surface dust emission rates. It is found that wind fields (both speed and direction) remain nearly identical when including boundary conditions. Likewise, two meter temperatures are only cooled slightly (on the order of 0.1°C) due to decreases of incoming surface shortwave radiation which is scattered/absorbed aloft due to dust increases. Lastly, to confirm that dust, itself, at the boundaries causes these changes, we examine the dust emission rates for all four tracers in both CONT and BC simulations. Given that wind fields remain similar, it is expected, and found, that the emission rates for all tracers are nearly identical between CONT and BC.

Additional work is completed in examining whether using a dust "climatology" is sufficient in representing mineral aerosols at the boundaries. That is, averaged monthly values are constructed from the five year data and then used to impose dust concentration values at the boundaries, identical to the nesting technique. Essentially, five year's worth of dust concentrations are averaged for each month to make one seasonal cycle of tracer mixing ratios. Results reveal that there is little difference in using actual mixing ratios compared to the climatology dataset. For example, similar increases in AOD (spatially and in magnitude) occur as well as changes in seasonality and tracer concentrations. Therefore, a climatology of dust concentrations (via observations or a global model) should yield results similar to the nesting technique described above. Although, it should be mentioned that 5 years worth of dust concentration values may not be enough to define an actual climatology; however, as shown, our results indicate that there are little fluctuations in year to year values in the boundary conditions themselves.

Lastly, it is important to note that our results can only confirm that over Southwest Asia, given our domain size, including dust concentrations at the boundaries improves RegCM3's performance in simulating dust loading. It is possible that over other regions this process is either not as important or that domain configuration sufficiently captures all dust sources. Nevertheless, this work highlights that dust at the boundaries of a regional climate model may be necessary in accurately simulating the dust loading over different regions. Likewise, including mineral aerosol boundary conditions may be an adequate substitute instead of increasing domain size to include dust sources far from the intended study region. Additionally, longer simulations should be performed to fully discern the effects of boundary conditions on the climatology of dust within the domain itself. In any case, it is confirmed that including mineral aerosols at the boundaries can have profound effects on dust loading over Southwest Asia.

References

Abdou WA, Diner DA, Martonchik JV, Bruegge CJ, Kahn RA, Gaitley BJ, Crean KA, Remer LA, Holben B (2005) Comparison of coincident multiangle imaging spectroradiometer and moderate resolution imaging spectroradiometer aerosol optical depths over land and ocean scenes containing aerosol robotic network sites. J Geophys Res 110:D10S07

Alfaro S, Gomes L (2001) Modelling mineral aerosol production by wind erosion: emission intensities and aerosol size distributions in source areas. J Geophys Res 106:18075–18084

Cakmur RV, Miller RL, Torres O (2004) Incorporating the effect of small-scale circulations upon dust emission in an atmospheric general circulation model. J Geophys Res 109:D07201

Davies H, Turner R (1977) Updating prediction models by dynamical relaxation: an examination of the technique. Quar J Am Meteorol Soc 103:225–245

Dickinson R, Henderson-Sellers A, Kennedy P (1993) Biosphere atmosphere transfer scheme (BATS) version 1e as coupled to the NCAR Community Climate Model. Technical report, National Center for Atmospheric Research

Giorgi F, Marinucci M, Bates G (1993) Development of a second generation regional climate model (regcm2). Part I: boundary layer and radiative transfer processes. Mon Weather Rev 121:2794–2813

Giorgi F, Marinucci M, Bates G, DeCanio G (1993) Development of a second generation regional climate model (regcm2). Part II: convective processes and assimilation of lateral boundary conditions. Mon Weather Rev 121:2814–2832

Giorgi F, Mearns L, Shields C, McDaniel L (1998) Regional nested model simulations of present day and 2xco2 climate over the Central Plains of the US. Clim Change 40:457–493

Grell G, Dudhia JJ, Stauffer D (1994) A description of the fifth-generation Penn State/NCAR Mesoscale Model (MM5), Technical Note TN-398+IA

Holtslag A, de Bruin E, Pan H (1990) A high resolution air mass transformation model for short-range weather forecasting. Mon Weather Rev 118:1561–1575

Kahn RA, Nelson D, Garay M, Levy R, Bull M, Diner D, Martonchik J, Paradise S, Hansen E, Remer L (2009) Misr aerosol product attributes and statistical comparisons with modis. Geosci Remote Sens 47:4095–4114

Kalnay E, Kanamitsu M, Kistler R, Collins W, Deaven D, Gandin L, Iredell M, Saha S, White G, Woollen J, Zhu Y, Leetmaa A, Reynolds B, Chelliah M, Ebisuzaki W, Higgins W, Janowiak J, Mo K, Ropelewski C, Wang J, Jenne R, Joseph D (1996) The NCEP/NCAR 40-year reanalysis project. Bull Am Meteorol Soc 77:437–471

Kiehl J, Hack J, Bonan G, Boville B, Breigleb B, Williamson D, Rasch PJ (1996) Description of the ncar community climate model (ccm3). Technical Note TN-420+STR, National Center for Atmospheric Research

Luo C, Mahowald N, del Corral J (2003) Sensitivity study of meteorological parameters on mineral aerosol mobilization, transport, and distribution. J Geophys Res 108:4447

Marcella MP, Eltahir EAB (2008) Modeling the hydroclimatology of Kuwait: the role of subcloud evaporation in semiarid climates. J Clim 21:2976–2989

Marcella MP, Eltahir EAB (2010) Effects of mineral aerosols on the summertime climate of southwest asia: Incorporating subgrid variability in a dust emission scheme. J Geophys Res D18203. doi:10.1029/2010DOI14036

Marticorena B, Bergametti G (1995) Modeling the atmospheric dust cycle, i, design of soil-derived dust emission scheme. J Geophys Res 100:16416–16430

Miller R, Tegen I (1998) Climate response to soil dust aerosols. J Clim 11:3247–3267

Pal J, Giorgi F, Bi X, Elguindi N, Solmon F, Gao X, Francisco A, andd Zakey R, Winter J, Ashfaq M, Syed F, Bell J, Diffenbaugh N, Karmacharya J, Konare A, Martinez-Castro D, Porfirioda Rocha R, Sloan L, Steiner A (2007) Regional climate modeling for the developing world: the ICTP RegCNET and RegCM. Bull Am Meteorol Soc 88:1395–1409

Pal J, Small E, Eltahir EAB (2000) Simulation of regional-scale water and energy budgets: representation of subgrid cloud and precipitation processes within RegCM. J Geophys Res 105:29579–29594

Prasad AK, Singh RP (2006) Comparison of misr-modi aerosol optical depth over the indo-gangetic basin during the winter and summer seasons (200-2005). Remote Sens Environ 107:109–119

Prospero JM, Ginoux P, Torres O, Nicholson E, Gill TE (2002) Environmental characterization of global sources of atmospheric soil dust identified with the Nimbus 7 total ozone mapping spectrometer (TOMS) absorbing aerosol product. Rev Geophys 40:1–29

Reynolds RW (2002) An improved in situ and satellite SST analysis for climate. J Clim 15:1609–1625

Sokolik IN, Winker DM, Bergametti G, Gillette DA, Carmichael G, Kaufman YJ, Gomes L, Schuetz L, Penner JE (2001) Introduction to special section: outstanding problems in quantifying the radiative impacts of mineral dust. J Geophys Res 106: 18015–18027

Solmon F, Mallet M, Elguindi N, Giorgi F, Zakey AS, Konare A (2008) Dust aerosol impact on regional precipitation over western Africa, mechanisms and sensitivity to absorption properties. Geophys Res Lett 35:L24705

Tegen I, Lacis AA (1996) Modeling of particle size distribution and its influence on the radiative properties of mineral dust aerosols. J Geophys Res 101:19237–19244

Tegen I, Miller RL (1998) A general circulation model study on the interannual variability of soil dust aerosol. J Geophys Res 103:25875–25995

Zakey A, Solmon F, Giorgi F (2006) Implementation and testing of a desert dust module in a regional implementation and testing of a desert dust module in a regional climate model. Atmos Chem Phys 6:4687–4704

Zeng X, Zhao M, Dickinson R (1998) Intercomparison of bulk aerodynamic algorithms for the computation of sea surface fluxes using TOGA coare and TAO data. J Clim 11:2628–2644

Zhang DF, Zakey AS, Gao XJ, Giorgi F, Solmon F (2009) Simulation of dust aerosol and its regional feedbacks over east asia using a regional climate model. Atmos Chem Phys 9:1095–1110